Motion-gated acquisition for *in vivo* optical imaging

Sylvain Gioux
Boston University
48 Cummington Street
Boston, Massachusetts 02215
and
Beth Israel Deaconess Medical Center
330 Brookline Avenue, Room SL-B05
Boston, Massachusetts 02215

Yoshitomo Ashitate
Merlijn Hutteman
John V. Frangioni
Harvard Medical School
Beth Israel Deaconess Medical Center
330 Brookline Avenue, Room SL-B05
Boston, Massachusetts 02215

Abstract. Wide-field continuous wave fluorescence imaging, fluorescence lifetime imaging, frequency domain photon migration, and spatially modulated imaging have the potential to provide quantitative measurements *in vivo*. However, most of these techniques have not yet been successfully translated to the clinic due to challenging environmental constraints. In many circumstances, cardiac and respiratory motion greatly impair image quality and/or quantitative processing. To address this fundamental problem, we have developed a low-cost, field-programmable gate array–based, hardware-only gating device that delivers a phase-locked acquisition window of arbitrary delay and width that is derived from an unlimited number of pseudo-periodic and nonperiodic input signals. All device features can be controlled manually or via USB serial commands. The working range of the device spans the extremes of mouse electrocardiogram (1000 beats per minute) to human respiration (4 breaths per minute), with timing resolution ⩽0.06%, and jitter ⩽0.008%, of the input signal period. We demonstrate the performance of the gating device, including dramatic improvements in quantitative measurements, *in vitro* using a motion simulator and *in vivo* using near-infrared fluorescence angiography of beating pig heart. This gating device should help to enable the clinical translation of promising new optical imaging technologies.
[DOI: 10.1117/1.3275473]

Keywords: optical imaging; gating; image-guided surgery; clinical translation; near-infrared (NIR) fluorescence.

Paper 09356R received Aug. 13, 2009; revised manuscript received Oct. 13, 2009; accepted for publication Oct. 20, 2009; published online Dec. 22, 2009.

1 Introduction

Over the past decade, wide-field, noncontact biomedical imaging has made tremendous progress toward solving relevant *in vivo* clinical problems. Straightforward techniques such as continuous wave (CW) fluorescence imaging have already been translated to the clinic and can provide surgeons with real-time guidance during surgical procedures.[1–7] More complex techniques employing time-varying sources and image collection have been used to image fluorescence lifetime and endogenous tissue optical properties [i.e., absorption (μ_a) and reduced scattering (μ_s') coefficients] *in vivo*, and over large fields of view (FOVs).[8–12] Spatially modulated (i.e., structured) illumination has also been successfully used to image tissue optical properties *in vivo*, and over large FOVs.[13–16] When combined with multiwavelength analysis, the imaging of optical properties can be used to characterize the biochemical composition of tissues and thus provide a useful tool for noncontact, wide-field tumor delineation.[17,18]

Although the results obtained using these techniques are quite promising, the field is still struggling with their translation into clinical environments. One problem of major impact to clinical translation is motion. This problem, also faced by other clinical imaging techniques such as magnetic resonance imaging (MRI), positron emission tomography (PET), computed tomography (CT), and optical coherence tomography (OCT), leads to random image location in space, impairs proper focusing, and generates blurred images when image acquisition time is long. This results in considerable error when performing qualitative localization of structures in a single image, and significant processing errors when applying quantitative techniques to a number of images acquired over time. For example, in the context of quantitative optical imaging, techniques such as fluorescence lifetime measurement and optical property extraction require that sequential images be acquired and co-registered in space. Not fulfilling co-registration renders the techniques unusable and prevents translation to a clinically realistic environment.

Several techniques have been developed to reduce motion-induced image noise, with most based on the acquisition and processing of physiological signals such as from the electrocardiogram (ECG) and/or plethysmograph (i.e., respiration). Solutions have been described and validated for MRI, CT, PET, and OCT.[19–23] Different approaches have been described for the processing of the acquired signal(s) and the generation of a reliable gating phase and are reviewed in Ref. 24. One such software solution was initially implemented by our group,[25] but did not provide the desired accuracy due to over-

Address all correspondence to: John V. Frangioni, Harvard Medical School, Beth Israel Deaconess Medical Center, 330 Brookline Avenue, Room SL-B05, Boston, Massachusetts 02215. Tel: 617-667-0692; Fax: 617-667-0981; E-mail: jfrangio@bidmc.harvard.edu.

1083-3668/2009/14(6)/064038/8/$25.00 © 2009 SPIE

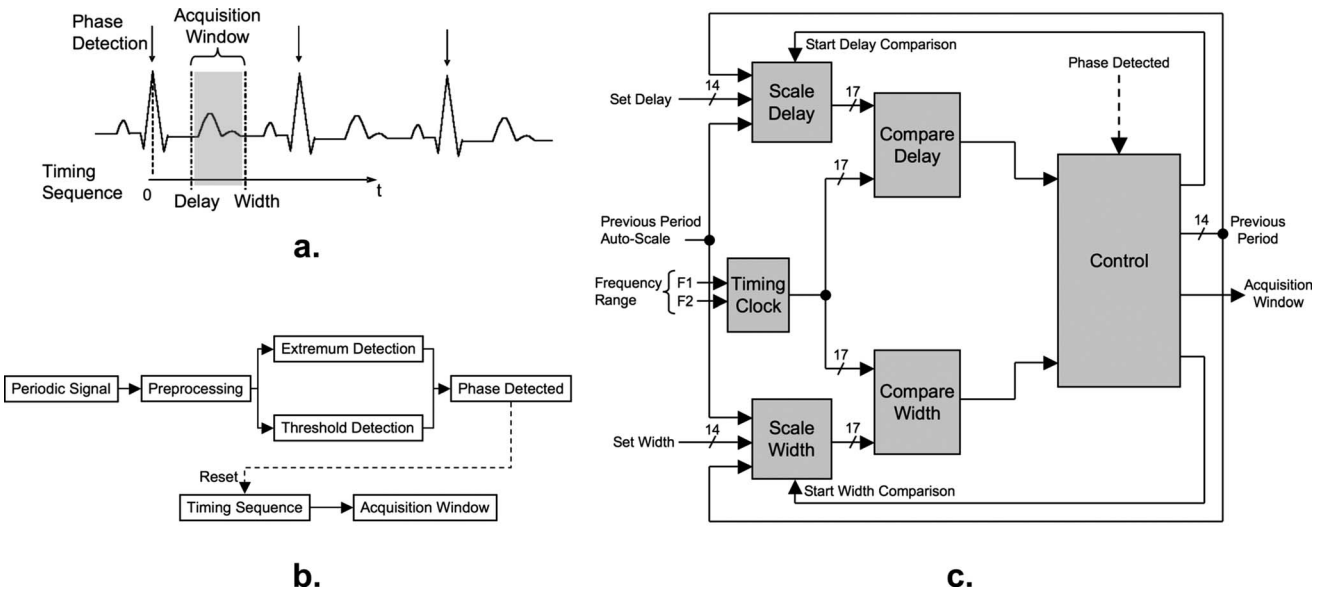

Fig. 1 Principles of the gating circuit. (a) Representative ECG tracing showing phase detection via the R wave of the QRS complex (arrows) and generation of an acquisition window of desired delay and width. (b) Flowchart of the gating circuit algorithm starting with a pseudo-periodic signal and ending with a precise acquisition window. (c) Overview of the timing sequence embedded in the field-programmable gate array (FPGA).

whelming of the processor with multiple camera streaming and computationally intensive signal processing. Other techniques involve the acquisition of several images at random times followed by postacquisition filtration to remove the undesired nonfocused images.[22,26] While this approach has its usefulness, it is obviously not suited for real-time qualitative and quantitative optical imaging. Hardware solutions are therefore preferred for real-time imaging. Although motion-gating capabilities are included in many commercially available MRI and CT systems, there are currently few off-the-shelf hardware devices available that could be used for *in vivo* optical imaging from mouse to human. Of special concern to *in vivo* optical imaging are the relatively long exposure times, usually greater than 100 ms for fluorescence, and the wide range of physiological frequencies ranging from human respiration ($\approx$0.1 Hz) to mouse heartbeat ($\approx$10 Hz).

In this study, we hypothesized that it should be possible to construct a hardware-only gating device that could accommodate all of the common pseudo-periodic and nonperiodic signals arising in a typical clinical environment and to produce a precise acquisition window compatible with any type of optical imaging application.

2 Materials and Methods

2.1 *Gating Algorithm and Circuit*

The gating algorithm was designed to provide a synchronized acquisition gate, or "acquisition window," derived from an incoming signal. Here, we describe the synchronized acquisition of images captured by a camera with respect to an incoming physiological signal. The physiological signal was assumed to be pseudo-periodic and directly linked to the motion of the image being acquired. Thus, one can use the previous period to predict the width of the following period. It was then possible to acquire the phase and period of the physiological input signal and to generate a user-controlled acquisition window in real time. Various techniques are available for performing this operation and are reviewed in Ref. 24 The most commonly used techniques are periodic threshold detection coupled with differentiation filtering, digital filters, or pattern recognition.

The following is an overview of the electronic circuit used by our gating device, with more detailed information available at www.frangionilab.org. First, the incoming analog signal ($\pm$10 V maximum) was conditioned using a precision differential instrumentation amplifier, low-pass filter, tunable high-pass filter, and tunable gain to provide $\pm$1 V to $\pm$4 V input to the circuit. Phase was then assessed through threshold detection and differentiation filtering. Threshold detection ensured that no other extrema were incorrectly identified as the phase of the signal. Threshold detection was also automatically scaled to the previous period's maximum to accommodate various types of incoming signals. It is important to note that a single-threshold approach does not guarantee a completely accurate time detection of the phase due to changes in the shape of the signal. The addition of a differentiation filter ensures an accurate and repeatable detection of the signal's phase by the means of extremum detection [in the case of ECG, the peak of the R wave in the QRS complex; Fig. 1(a)]. Last, the threshold and extremum detection signals were combined together into a single transistor-transistor logic (TTL) pulse per period indicative of the incoming signal's phase. The phase pulse was then used to reset a timing sequence, which controls the delay and width of the acquisition window [Figs. 1(a) and 1(b)].

The timing sequence was generated using a field-programmable gate array (FPGA; Xilinx Spartan 3AN). The schematic of the timing sequence within the FPGA (programmed by the Boston University Electronics Design Facility, Boston, Massachusetts) is shown in Fig. 1(c). The phase detection pulse was used to launch a timing sequence generated by a user-controlled timing clock. In order to accommo-

date a wide range of signal frequencies with high timing accuracy, two 14-bit counters were used: one defining the start of the acquisition window (referred to as the "delay" relative to the phase signal) and the other defining the end of the acquisition window (referred to as the "width"). The desired delay and width could be entered as absolute values, representative of the units of the timing clock, or could be scaled automatically as a percentage of the previous period. The latter assumes that signal period and physical displacement are proportional, which permits compensation for variability in frequency (e.g., with respiration), as can occur with a normal ECG. The final acquisition window was a jumper-selectable TTL or complementary metal-oxide semiconductor (CMOS)-compatible pulse.

Gating device components were from DigiKey (Thief River Falls, Minnesota) and Mouser (Mansfield, Texas). Four-layer printed circuit boards (PCBs) were fabricated by Nashua Circuits (Nashua, New Hampshire) and assembled by Sure Design (Farmingdale, New Jersey). Gerber files for PCB manufacturing, a parts list, assembly instructions, and a user manual are available at www.frangionilab.org.

2.2 *In Vitro Validation Experiments*

We performed two types of *in vitro* validation of the gating device. Electrical validation was performed to test production of a reliable acquisition window from one or more periodic input signals, while functional validation was performed to test camera acquisition of an image in cyclic motion.

Input signals were generated using a Hewlett Packard (HP) model HP3245A dual-channel signal generator. One channel was used to produce a higher frequency triangular wave (e.g., ECG-like) with frequency f, 1-V peak-to-peak (Vpp), and 10% duty cycle, while the other was used to produce a lower frequency sine wave (e.g., plethysmograph-like) with frequency $f/10$, 250 mVpp, and 50% duty cycle. The lower frequency signal was also added to the higher frequency signal using a model ZFRSC-42 voltage combiner (Mini-Circuits, Brooklyn, New York) to simulate the type of slow baseline drift typically seen in clinical tracings. Testing frequencies f ranged from 60 to 600 beats per minute (bpm). Circuit inputs and outputs were monitored using a LeCroy WaveSurfer 44Xs, 400-MHz (2.5 GS/s) digital oscilloscope. Power for the gating device was provided by a ± 12-V, +5-V model WM220-1 (Elpac, Irvine, California) power supply.

To test functionality of the gating device, we constructed a motion simulator capable of moving an optical phantom using an arbitrary analog voltage input. The motion simulator consisted of a custom vertical translation stage (Microvideo Instruments, Avon, Massachusetts) that could be tilted to produce x, y, and z motion, a model VL23-020D-ZAA DC servo motor (Applied Motion, Watsonville, California), and a model BLU-200 (Applied Motion) motor controller. Gated image acquisition was performed on a single PC with the acquisition window triggering a National Instruments (Austin, Texas) PCI-6229 multifunction board. Images were acquired, displayed, and saved using custom LabView software (National Instruments) capable of simultaneously acquiring two Firewire cameras [color and near-infrared (NIR) fluorescence] with triggering from the multifunction board. The cameras used were an Imitech (Seoul, Korea) IMC-80F for color video and a Hamamatsu (Bridgewater, New Jersey) Orca-AG for NIR fluorescence. Cameras were mounted to custom optics as described in detail previously.[27] Color camera exposure time was 67 msec and NIR camera exposure time was 100 ms. The optical phantom consisted of a 384-well plate (85 mm $\times$ 130 mm) filled with either 10 μM indocyanine green (ICG; NIR fluorescent) in dimethylsulfoxide or 2% skim milk (visible with color camera). White (400 to 650 nm) and 760 nm NIR fluorescence excitation light was provided by custom LED modules.[28]

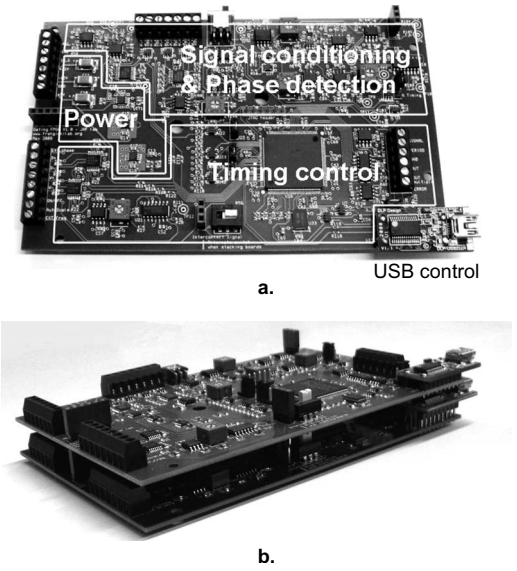

Fig. 2 Stackable gating devices. (a) Single assembled gating device showing major functions of the PCB as well as the USB control port. (b) Two stacked gating devices for use in ANDing two different, dephased input signals to provide a single image acquisition window.

2.3 *In Vivo Validation Experiments*

In vivo validation of the device was performed during NIR fluorescence angiography of the beating swine heart using intravenously injected ICG (0.014 mg/kg per injection) as the contrast agent. Animals were studied under the supervision of an approved institutional protocol. Yorkshire pigs ($n=3$) weighing 30 kg and of either sex were purchased from E. M. Parsons and Sons (Hadley, Massachusetts). Anesthesia was induced using 4.4 mg/kg intramuscular Telazol (Fort Dodge Labs, Fort Dodge, Iowa), and maintained through a 7-mm endotracheal tube with 1.5% isoflurane/balance O_2 at 5 L/min. The heart was exposed for imaging by a midline sternotomy. After each study, anesthetized pigs were euthanized by rapid intravenous injection of 10 ml of Fatal-Plus (Vortech Pharmaceuticals, Dearborn, Michigan).

The ECG signal was obtained through standard three-lead electrodes attached to a Datex/Ohmeda model S/5 vital signs monitor. The acquisition window from the gating device was used to trigger image acquisition by custom LabView software. Color camera exposure time was 67 msec, and NIR camera exposure time was 100 ms. Color and NIR images were acquired with gating on and off, and regions of interest

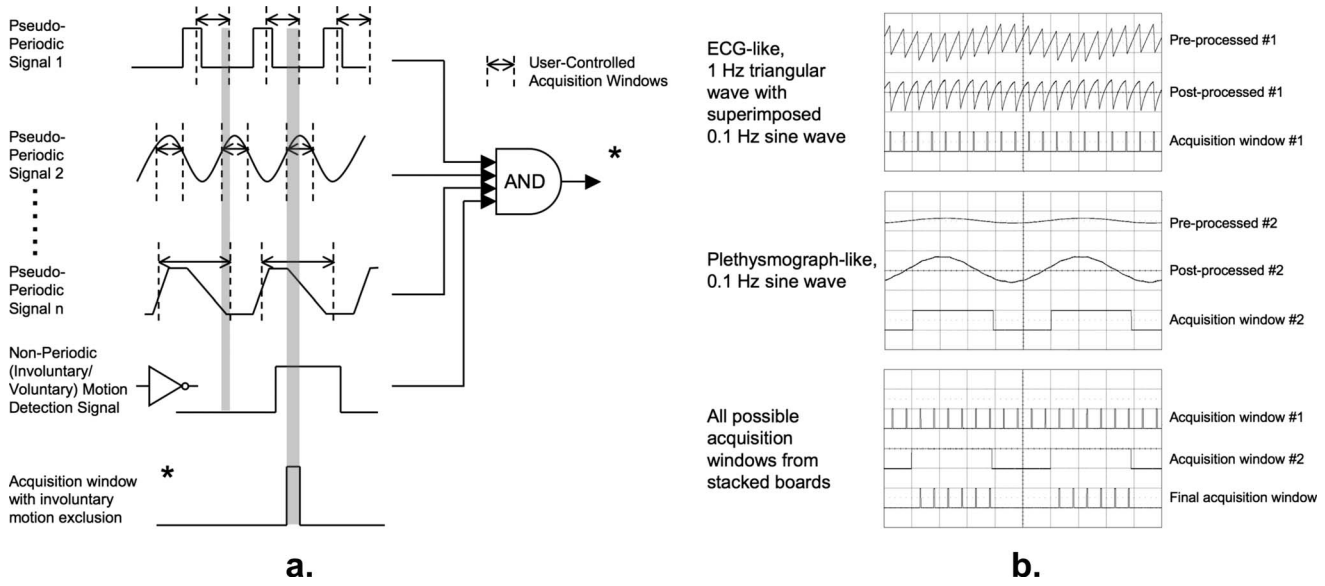

Fig. 3 Accommodation of multiple periodic and nonperiodic input signals by the gating circuit. (a) Schematic showing *n* pseudo-periodic input signals combined with a nonperiodic input signal to provide a single image acquisition window of any desired delay and width. Note that the nonperiodic input signal, for example, from an accelerometer detecting involuntary or voluntary motion, may have to be inverted prior to the logical AND. The image acquisition window is a TTL-or CMOS-compatible pulse. (b) Electrical validation of the gating device. Shown are a 1-Hz, 1-Vpp triangular wave of 10% duty cycle (ECG-like signal) with a superimposed 0.1-Hz, 250-mVpp sine wave (plethysmograph-like) of 50% duty cycle (top); a 0.1-Hz, 250-mVpp sine wave (plethysmograph-like) of 50% duty cycle (middle); and the logical AND of acquisition windows from each (bottom).

over the left anterior descending artery and the great cardiac vein were quantified over time for NIR fluorescence intensity.

3 Results

3.1 *Gating Device*

An assembled gating device is shown in Fig. 2(a). The assembled PCB could be mounted in an enclosure, controlled via manual switches, and operated as a stand-alone device or operated in a fully automated fashion using the integrated USB port. Indeed, the gating device was designed with dimensions of 14.5 cm W × 9 cm D × 1.5 cm H, permitting up to two stacked devices to be mounted in a CA-1000 enclosure (National Instruments) and thus connected seamlessly to a multifunction board. The total price for a single prototype device was $1,000, which included $200 for board fabrication, $300 for components, and $500 for manual board assembly. When manufactured in larger quantities, the price per device fell to less than $300.

To produce a single acquisition window from multiple simultaneous signals, such as from simultaneous cardiac and respiratory gating, devices were designed to be stackable [Fig. 2(b)]. When stacked, the acquisition window from the lowest device in the stack outputs the logical AND of the acquisition windows from all gating devices above it [Fig. 3(a)], although individual acquisition windows are also available if needed. Each stacked device has its own selectable input frequency range (Table 1) chosen from 4 to 40 cycles per minute (cpm), 25 to 250 cpm, and 100 to 1000 cpm. These frequency ranges cover the entire spectrum from mouse ECG to human plethysmograph. In addition, each board has a TTL- and CMOS-compatible input to suppress the acquisition win-

Table 1 Setting the gating circuit frequency range based on the species of interest and source of motion-induced noise.

Frequency range selection (F1F2 bits)	Working range (cycle per minute)	Species	Signal type
00	(4–40 cpm)	Large animal/human	Respiration
01	(25–250 cpm)	Large animal/human	ECG
		Rodent	Respiration
10	(100–1000 cpm)	Rodent	ECG

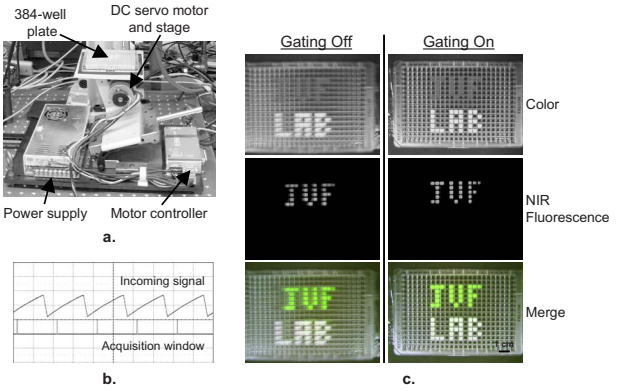

Fig. 4 *In vitro* validation of the gating device using simultaneous color video and NIR fluorescence imaging. (a) DC servo motor–based motion simulator with moving stage. (b) 1-Hz, 2-Vpp triangular wave of 10% duty cycle (ECG-like signal) used to drive the motion simulator. Desired acquisition window is also indicated. (c) Real-time imaging of a 384-well plate having wells filled with visibly white (the word "Lab") or NIR fluorescent (the word "JVF") liquid and placed on the motion simulator stage. Shown are the color image (top), NIR fluorescence image (middle), and pseudo-colored (lime green) merge of the two (bottom) in the absence (left) and presence (right) of gating, as described in Fig. 4(b). (Color online only.)

dow in the setting of nonperiodic signals, such as from involuntary or voluntary muscle movement detected using an accelerometer [Fig. 2(a)]. As suggested in the figure, such signals might need to be inverted depending on the sensor output.

3.2 *In Vitro Validation Experiments*

By selecting the appropriate frequency range (Table 1), we tested operation of the gating device with input frequencies from 4 to 1000 cycles per minute (cpm). Electrical outputs from a typical experiment are shown in Fig. 3(b). Notice that a feature built into the circuit is the ability to remove slow baseline drift during signal processing. For each type of input signal, a stable and reliable acquisition window could be generated and ANDed to produce an acquisition window that fit multiple criteria. For all frequency ranges, timing resolution was $\leqslant$0.06%, and jitter was $\leqslant$0.008% of the input signal's period. This high precision was the result of employing a 17-bit timing clock and 14-bit counters within the FPGA, which reduced synchronization jitter between the phase pulse and timing clock.

To simulate a beating heart, a motion simulator [Fig. 4(a)] that moves a stage vertically and laterally in response to an analog signal was constructed. To simulate an ECG, the input signal was a 1-Hz triangular wave of 2 Vpp and 10% duty cycle [Fig. 4(b)]. As shown in Fig. 4(c) and Video 1 and 2 (gating off and gating on, respectively), the gating device dramatically improved both color video and NIR fluorescence image acquisition. Indeed, with gating on, the images appeared crisp, co-registered, and motionless except for an occasional slight phase shift due to software overhead.

3.3 *In Vivo Validation Experiments*

The beating heart of a 35-kg pig is the closest approximation to a human heart and represents a worst case scenario for optical imaging since each systole results in over 3 cm of vertical, lateral, and horizontal displacement. Nevertheless, as shown in Fig. 5 (top) and Videos 3 and 4 (gating off and gating on, respectively), the gating device was able to "freeze" image acquisition during NIR fluorescence angiography such that even the smallest arteries and veins were visible and could be imaged as if they were immobile. In fact, the only blurring that occurred was the result of the 100-msec exposure time necessary for NIR fluorescence imaging.

Importantly, in addition to qualitative improvements in optical imaging, the gating device also enabled quantitation of the NIR fluorescence signal emanating from the arteries and veins of the heart. Shown in Fig. 5 (bottom) is the ratio of the NIR fluorescence signal arising from the left anterior descending coronary artery and the great cardiac vein. In the absence of gating, considerable noise exists in this measurement due to blurring and is seen as a 1.2-Hz signal of $\approx$5% standard deviation superimposed on the artery/vein ratio. However, in the presence of gating, the noise of the measurement is reduced to $<$2% standard deviation, and the various phases of vascular filling can be identified readily without interference from the heartbeat.

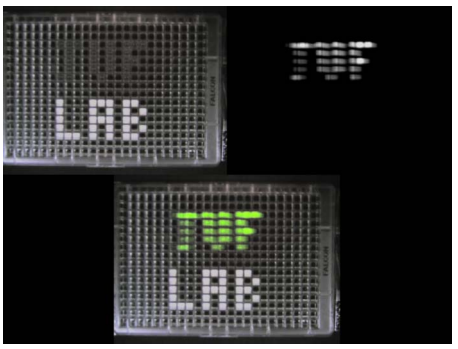

Video 1 Real-time imaging of a 384-well plate having wells filled with visibly white (the word "Lab") or NIR fluorescent (the word "JVF") liquid and placed on the motion simulator stage. Shown are the color image (top left), NIR fluorescence image (top right), and pseudo-colored (lime green) merge of the two (bottom) in the absence of gating (see Fig. 4). (Color online only.) (QuickTime, 1.81 MB). [URL: http://dx.doi.org/10.1117/1.3275473.1].

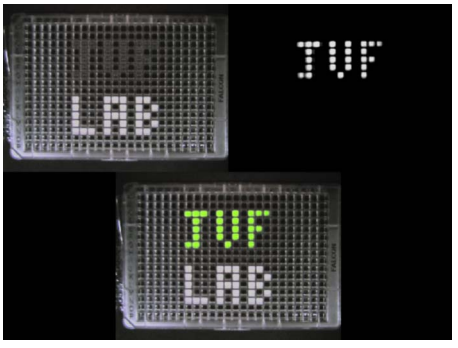

Video 2 Same as Video 1, but in the presence of gating (see Fig. 4). (QuickTime, 730 KB). [URL: http://dx.doi.org/10.1117/1.3275473.2]

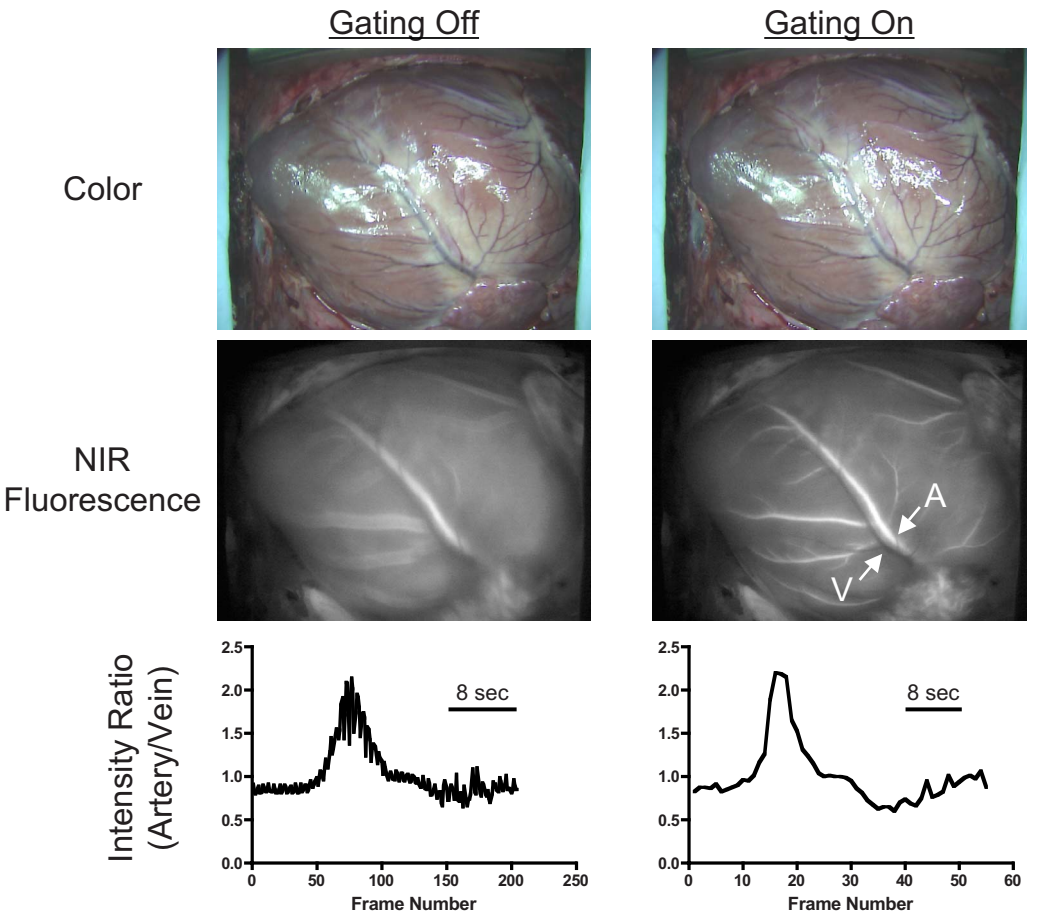

Fig. 5 *In vivo* validation of gating device performance using the beating heart of a pig. Shown is NIR fluorescence angiography using 0.014 mg/kg ICG injected intravenously with gating off (left) or gating on (right). In addition to color video images (top) and NIR fluorescence images (middle), the NIR fluorescence pixel intensity ratios of the left anterior descending coronary artery (A) to the great cardiac vein (V) are also shown (bottom). NIR fluorescence images have identical exposure times and normalizations.

4 Discussion

The gating device we describe in this study has been shown to provide reliable and stable acquisition windows from one or more pseudo-periodic input signals. Although the device adapts for slow changes in period and amplitude, fast and large variations in period render the incoming signal nonperiodic and thus not interpretable to the device. Special care should be given to deliver a clean, spike-free analog input signal by avoiding moving the electrode wires, or using electrocautery, during gated image acquisition. Additional software modifications can also be used to automate frequency

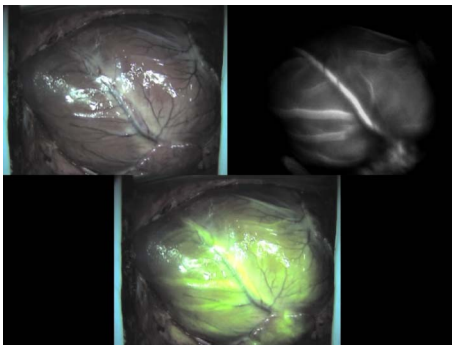

Video 3 *In vivo* validation of gating device performance using the beating heart of a pig. Shown is NIR fluorescence angiography using 0.014 mg/kg ICG injected intravenously. Shown are the color image (top left), NIR fluorescence image (top right), and pseudo-colored (lime green) merge of the two (bottom) in the absence of gating (see Fig. 5) (Color online only.) (QuickTime, 4.98 MB).
[URL: http://dx.doi.org/10.1117/1.3275473.3].

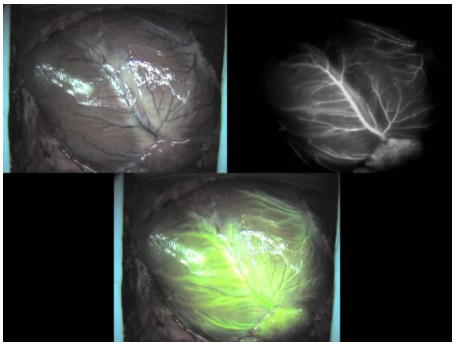

Video 4 Same as Video 3, but in the presence of gating (see Fig. 5) (QuickTime, 2.35 MB).
[URL: http://dx.doi.org/10.1117/1.3275473.4].

range and gain selection via the TTL error signals provided by the device.

As described earlier, the gating device accommodates slow periodic variations by stretching the acquisition window proportionally to the incoming signal's prior period. This approach assumes that the electrical signal and mechanical motion stretch proportionally with period, a reasonable assumption with respect to electrophysiological signals such as ECG and respiration.

One critical point when using the gating device is optimization of the camera acquisition software. The simple LabView code used in this study was not able to acquire two or more cameras with perfect simultaneity, which resulted in occasional phase shifts and image blurring. Newer software developed for our Fluorescence-Assisted Resection and Exploration [FLARE™] image-guided surgery system is capable of truly simultaneous acquisition of up to three Firewire cameras[7] and is expected to solve this problem. Whenever possible, camera exposure time should be as short as possible relative to the physiological signal period (typically lower than 10%), which will help eliminate blurring and improve quantitation. Stacked gating devices and multiple input signal ANDing can also help reduce noise by removing superimposed mechanical motions. Last, hardware triggering of camera acquisition using the gating device window status bit (1: acquire; 0: do not acquire) is always preferred. Using this mode, motion-gated imaging is limited only by the minimum ($\approx 10\ \mu s$) exposure time of a typical NIR camera (e.g., Hamamatsu ORCA C4742-80-12AG) since the gating device provides a timing resolution $\leqslant 0.06\%$ and a jitter $\leqslant 0.008\%$ of the input signal's period. In all circumstances, it is the camera readout time (15 fps for the ORCA with 2×2 binning) that will be rate limiting.

This study will hopefully contribute to the clinical translation of real-time quantitative optical imaging techniques that are now limited by periodic or pseudo-periodic motion artifacts. For example, as fast parallel computing of image pixels using graphics processing units (GPUs) becomes more commonplace, CCD camera acquisition becomes the critical parameter for permitting real-time imaging. Motion-free acquisition of these images should enable improved quantitation.

We envision that the gating device could be employed to improve quantitation of virtually any optical imaging methodology. One technology that could benefit immediately is NIR fluorescence for image-guided surgery. Although this technique has already been translated to the clinic,[1–7] it is presently limited by the harsh mechanical motions encountered in the operating room. These include those caused by the beating heart, ventilated chest, and inadvertent "bumps" from caregivers. The stackable gating device we describe can suppress all such contributors to image noise since an unlimited number of pseudo-periodic and nonperiodic signals can be combined to control the acquisition window, greatly improving the visualization of fine structures of interest. It should also be emphasized that no part of the human body is immune from physiological motion, and that every surface of the body, including the toes, moves a perceptible and measurable distance with every heartbeat. The higher the resolution and narrower the depth of field of the optical imaging technique employed, the more such movement contributes to image noise.

Gated acquisition might also be useful for contact point measurements. Since point measurements can be influenced by applied pressure[29] and blood volume effects due to pulsatile arterial flow, the combination of both motion gating for heartbeat and pressure-level gating using the gating device's provided nonperiodic signal input could improve noise reduction in such measurements.

Last, our gating device is not limited to the field of biomedical optics since it provides considerable versatility for use in most synchronized acquisition measurements. For example, processing filters can be changed during assembly to accommodate other types of periodic signals, phase detection can be provided externally as needed, and timing clock frequency can be changed within the FPGA code or provided externally (see www.frangionilab.org).

5 Conclusion

We have developed a low-cost, computer-controlled, and stackable gating device that permits an unlimited number of pseudo-periodic and nonperiodic signals to be combined to generate a precision acquisition window for optical imaging and image-guided surgery. Performance of the device has been validated *in vitro* using the extremes of frequency encountered during small animal imaging and image-guided surgery, and *in vivo* using beating hearts that match the electrical, mechanical, and optical properties of humans.

Acknowledgments

We thank Jerome Mertz (Boston University Department of Biomedical Engineering) for many helpful discussions; Eric Hazen and Paul Bohn (Boston University Electronics Design Facility) for FPGA programming; Summer L. Gibbs-Strauss, Aya Matsui, and Rita Laurence (Beth Israel Deaconess Medical Center) for assistance with animal experiments; Summer L. Gibbs-Strauss for editing; Jim Cuthbertson (Nashua Circuits) for PCB fabrication; Ken Thomas and Fernando Irizarry (Sure Design) for PCB assembly; Mike Paszak and Victor Laronga (Microvideo Instruments) for construction of the motion simulator; and Eugenia Trabucchi and Lorissa A. Moffitt for administrative assistance. This work was supported by NIH Grant No. R01-CA-115296 to Dr. Frangioni.

References

1. M. Fujiwara, T. Mizukami, A. Suzuki, and H. Fukamizu, "Sentinel lymph node detection in skin cancer patients using real-time fluorescence navigation with indocyanine green: preliminary experience," *J. Plast. Reconstr. Aesthet. Surg* **62**, e373–378 (2008).
2. T. Kitai, T. Inomoto, M. Miwa, and T. Shikayama, "Fluorescence navigation with indocyanine green for detecting sentinel lymph nodes in breast cancer," *Breast Cancer Res. Treat* **12**, 211–215 (2005).
3. M. Kusano, Y. Tajima, K. Yamazaki, M. Kato, M. Watanabe, and M. Miwa, "Sentinel node mapping guided by indocyanine green fluorescence imaging: a new method for sentinel node navigation surgery in gastrointestinal cancer," *Dig. Surg.* **25**, 103–108 (2008).
4. I. Miyashiro, N. Miyoshi, M. Hiratsuka, K. Kishi, T. Yamada, M. Ohue, H. Ohigashi, M. Yano, O. Ishikawa, and S. Imaoka, "Detection of sentinel node in gastric cancer surgery by indocyanine green fluorescence imaging: comparison with infrared imaging," *Ann. Surg. Oncol.* **15**, 1640–1643 (2008).
5. Y. Ogasawara, H. Ikeda, M. Takahashi, K. Kawasaki, and H. Doihara, "Evaluation of breast lymphatic pathways with indocyanine green fluorescence imaging in patients with breast cancer," *World J. Surg.* **32**, 1924–1929 (2008).
6. R. Sharma, W. Wang, J. C. Rasmussen, A. Joshi, J. P. Houston, K. E.

Adams, A. Cameron, S. Ke, S. Kwon, M. E. Mawad, and E. M. Sevick-Muraca, "Quantitative imaging of lymph function," *Am. J. Physiol. Heart Circ. Physiol.* **292**, H3109–3118 (2007).
7. S. L. Troyan, V. Kianzad, S. L. Gibbs-Strauss, S. Gioux, A. Matsui, R. Oketokoun, L. Ngo, A. Khamene, F. Azar, and J. V. Frangioni, "The FLARE™ intraoperative near-infrared fluorescence imaging system: a first-in-human clinical trial in breast cancer sentinel lymph node mapping," *Ann. Surg. Oncol.* **16**, 2943–2952 (2009).
8. J. R. Lakowicz and K. W. Berndt, "Lifetime-selective fluorescence imaging using an rf phase-sensitive camera," *Rev. Sci. Instrum.*. **62**, 1727–1734 (1991).
9. M. A. O'Leary, D. A. Boas, X. D. Li, B. Chance, and A. G. Yodh, "Fluorescence lifetime imaging in turbid media," *Opt. Lett.* **21**, 158–160 (1996).
10. J. S. Reynolds, T. L. Troy, and E. M. Sevick-Muraca, "Multipixel techniques for frequency-domain photon migration imaging," *Biotechnol. Prog.* **13**, 669–680 (1997).
11. J. S. Reynolds, T. L. Troy, R. H. Mayer, A. B. Thompson, D. J. Waters, K. K. Cornell, P. W. Snyder, and E. M. Sevick-Muraca, "Imaging of spontaneous canine mammary tumors using fluorescent contrast agents," *Photochem. Photobiol.* **70**, 87–94 (1999).
12. I. Munro, J. McGinty, N. Galletly, J. Requejo-Isidro, P. M. Lanigan, D. S. Elson, C. Dunsby, M. A. Neil, M. J. Lever, G. W. Stamp, and P. M. French, "Toward the clinical application of time-domain fluorescence lifetime imaging," *J. Biomed. Opt.* **10**, 051403 (2005).
13. A. Kienle, L. Lothar, M. S. Patterson, H. Raimund, R. Steiner, and B. Wilson, "Spatially resolved absolute diffuse reflectance measurements for noninvasive determination of the optical scattering and absorption coefficients of biological tissues," *Appl. Opt.* **35**, 2304–2314 (1996).
14. N. Dognitz and G. Wagnieres, "Determination of tissue optical properties by steady-state spatial frequency-domain reflectometry," *Lasers Med. Sci.* **13**, 55–65 (1998).
15. D. J. Cuccia, F. Bevilacqua, A. J. Durkin, F. R. Ayers, and B. J. Tromberg, "Quantitation and mapping of tissue optical properties using modulated imaging," *J. Biomed. Opt.* **14**, 024012 (2009).
16. S. Gioux, A. Mazhar, D. J. Cuccia, A. J. Durkin, B. J. Tromberg, and J. V. Frangioni, "Three-dimensional surface profile intensity correction for spatially modulated imaging," *J. Biomed. Opt.* **14**, 034045 (2009).
17. J. B. Fishkin, O. Coquoz, E. R. Anderson, M. Brenner, and B. J. Tromberg, "Frequency-domain photon migration measurements of normal and malignant tissue optical properties in a human subject," *Appl. Opt.* **36**, 10–20 (1997).
18. A. Cerussi, N. Shah, D. Hsiang, A. Durkin, J. Butler, and B. J. Tromberg, "*In vivo* absorption, scattering, and physiologic properties of 58 malignant breast tumors determined by broadband diffuse optical spectroscopy," *J. Biomed. Opt.* **11**, 044005 (2006).
19. M. A. Smith, J. P. Ridgway, J. W. Brydon, M. Been, R. H. Douglas, D. M. Kean, A. L. Muir, and J. J. Best, "ECG-gated T1 images of the heart," *Phys. Med. Biol.* **31**, 771–778 (1986).
20. Q. Yuan, L. Axel, E. H. Hernandez, L. Dougherty, J. J. Pilla, C. H. Scott, V. A. Ferrari, and A. S. Blom, "Cardiac-respiratory gating method for magnetic resonance imaging of the heart," *Magn. Reson. Med.* **43**, 314–318 (2000).
21. Y. Yang, S. Rendig, S. Siegel, D. F. Newport, and S. R. Cherry, "Cardiac PET imaging in mice with simultaneous cardiac and respiratory gating," *Phys. Med. Biol.* **50**, 2979–2989 (2005).
22. C. E. Woodhouse, W. R. Janowitz, and M. Viamonte Jr., "Coronary arteries: retrospective cardiac gating technique to reduce cardiac motion artifact at spiral CT," *Radiology* **204**, 566–569 (1997).
23. M. W. Jenkins, O. Q. Chughtai, A. N. Basavanhally, M. Watanabe, and A. M. Rollins, "*In vivo* gated 4D imaging of the embryonic heart using optical coherence tomography," *J. Biomed. Opt.* **12**, 030505 (2007).
24. B. U. Kohler, C. Hennig, and R. Orglmeister, "The principles of software QRS detection," *IEEE Eng. Med. Biol. Mag.* **21**, 42–57 (2002).
25. S. Gioux, A. M. De Grand, D. S. Lee, S. Yazdanfar, and J. V. Frangioni, "Improved optical sub-systems for intraoperative near-infrared fluorescence imaging," *Proc. SPIE* **6009**, 60090C (2009).
26. M. Gargesha, M. W. Jenkins, D. L. Wilson, and A. M. Rollins, "High temporal resolution OCT using image-based retrospective gating," *Opt. Express* **17**, 10786–10799 (2009).
27. E. Tanaka, H. S. Choi, H. Fujii, M. G. Bawendi, and J. V. Frangioni, "Image-guided oncologic surgery using invisible light: completed pre-clinical development for sentinel lymph node mapping," *Ann. Surg. Oncol.* **13**, 1671–1681 (2006).
28. S. Gioux, V. Kianzad, R. Ciocan, S. Gupta, R. Oketokoun, and J. V. Frangioni, "High power, computer-controlled, LED-based light sources for fluorescence imaging and image-guided surgery," *Mol. Imaging* **8**, 156–165 (2009).
29. R. Reif, M. S. Amorosino, K. W. Calabro, O. A'Amar, S. K. Singh, and I. J. Bigio, "Analysis of changes in reflectance measurements on biological tissues subjected to different probe pressures," *J. Biomed. Opt.* **13**, 010502 (2008).